https://doi.org/10.15407/ufm.23.01.090

**J.M. WINDAJANTI [1,*], M.S. RAJAPADNI [1], D.J.D.H. SANTJOJO [1], M.A. PAMUNGKAS [1], A. ABDURROUF [1], and T. AIZAWA [2,**]**

[1]Physics Department, Faculty of Mathematics and Natural Sciences,
Brawijaya University,
Jalan Veteran Malang, East Java, Indonesia
[2]Surface Engineering Design Laboratory,
Shibaura Institute of Technology,
Ota-City, Tokyo, Japan

* windajanti_jm@student.ub.ac.id, ** taizawa@sic.shibaura-it.ac.jp

# ANISOTROPIC PHASE TRANSFORMATION MECHANISM ON COARSE-GRAINED AND FINE-GRAINED PURE TITANIUM AT LOW-TEMPERATURE PLASMA NITRIDING

The nitriding process of the coarse-grained and fine-grained pure titanium proceeded by multidirectional forging technique has been investigated at temperatures of 623, 673, and 723 K. The process was carried out by high-density radiofrequency-direct current plasma combined with a rectangular hollow cathode device. The result obtained is a significant increase in surface hardness with increasing holding temperature. The surface hardness increases due to forming a surface layer composed of δ-$Ti_2N$, ε-$Ti_2N$, and $Ti_xN_x$ observed from x-ray diffraction results. This paper explains the mechanism of surface layer formation. We also observed anisotropic phase transformation of titanium nitride through the right shift of the x-ray diffraction peaks. Diffused nitrogen atoms during the nitriding process cause a change in crystal orientation through structural transformation of the metastable δ-$Ti_2N$ to the stable ε-$Ti_2N$. The structural reconstruction will continue by forming $Ti_xN_x$ to achieve stoichiometric equilibrium. More compacting of the surface microstructure is also obtained by increasing nitriding temperature.

**Keywords:** plasma nitriding, low temperature, pure titanium, fine-grained, anisotropic phase transformation.

Citation: J.M. Windajanti, M.S. Rajapadni, D.J.D.H. Santjojo, M.A. Pamungkas, A. Abdurrouf, and T. Aizawa, Anisotropic Phase Transformation Mechanism on Coarse-Grained and Fine-Grained Pure Titanium at Low Temperature Plasma Nitriding, *Progress in Physics of Metals*, **23**, No. 1: 90–107 (2022)

## 1. Introduction

Commercially pure titanium (Cp-Ti) is superior implant material due to its excellent biocompatibility, especially the osseointegration capability [1, 2]. In addition, this material also exhibits high toughness and corrosion resistance to be used as an orthopaedic implant. However, an implant material from Cp-Ti still suffers from high abrasive and adhesive wear due to its relatively low hardness and high friction coefficient [3–7].

Titanium properties could improve by the severe plastic deformation (SPD) processes. Several SPD techniques have been successfully developed for grain refinement in Cp-Ti, such as equal channel angular pressing [8], high-pressure torsion [9], severe shot peening [10], hydrostatic extrusion [11], twist extrusion [12], accumulative roll bonding [13], cryorolling [14], and high-ratio differential speed rolling [15], friction stir processing [16], and multidirectional forging (MDF) [1, 17].

A plasma nitriding process can increase wear and corrosion resistance [18]. In addition, the surface roughness is decreased by this process to lower the friction coefficient [2]. In particular, a low-temperature plasma nitriding is recently high-lighted to harden the pure titanium and titanium alloys without heat treatment effects [5]. The nitride la-yer formed by plasma nitriding comprises the face-centred cubic δ-TiN phase and the tetragonal ε-$Ti_2N$ phase. Beneath these compound layers, a nitrogen-rich α-Ti solid solution is formed by diffusion. The $TiN_x$ la-yer is formed by a reorganization of nitrogen atoms from the α-Ti solid solution and the ε-$Ti_2N$ phase [19, 20].

Fouquet *et al.* [18] reported that a radiofrequency (RF) plasma nitriding system was utilized to nitride Ti–6Al–4V alloy and that the $TiN_x$ layer acted as a diffusion barrier for nitrogen. The diffusion coefficient of nitrogen into the titanium matrix reduced by two orders of magnitude ($D_N^{TiN} = 3.95 \cdot 10^{-13}$ cm$^2$/s and $D_N^{Ti} = 1.81 \cdot 10^{-11}$ at 850 °C) [18, 21]. This unavoidable limitation resulted in the thin thickness of the nitride layer at a relatively low temperature and for a short processing time without change in the nitriding process. The fine-grained structure plays to accelerates the nitrogen diffusion over the grain boundaries and solves this limitation [10, 22].

In the present study, we carried out a combination of the nitriding process and fine-grained MDF structure. The Cp-Ti grade 2, with the coarse-grained size and the fine-grained size, preceded by the MDF technique, was nitrided by high-density radiofrequency-direct-current (RF–DC) plasma treatment. The nitriding process is carried out at relatively low temperatures at 623 K, 673 K, and 723 K by enlarging the plasma intensity using a rectangular hollow cathode placed on the cathode plate. The growth mechanism of $Ti_2N$ and TiN formation and nitrided layer thickness during plasma nitriding on the coarse-grained and fine-grained samples compared as a temperature function.

## 2. Experimental Methods

The nitriding process sample is a commercially pure titanium (Cp–Ti grade 2) plate with Ti 99.2 mas.%, C < 0.1 mas.%, Fe < 0.3 mas.%, H < 0.015 mas.%, N < 0.03 mas.%, and O < 0.25 mas.% after ASM material datasheet. Using electro-discharge machining (EDM) wire, these Cp–Ti plates were cut into a 20 mm (20 mm × 0.5 mm) rectangular specimen. The workpiece was cleaned using an alkaline solution in an ultrasosonic cleaning system for 1200 s, rinsed with water, and dried with ethanol.

The specimen was placed in a rectangular hollow cathode in the setup, as shown in Fig. 1; then, the specimen set was inserted into the chamber of the plasma nitriding system [23]. The nitridation was carried out by using the RF–DC plasma at 2 MHz. After specimens were placed in a rectangular hollow cathode into the setup, the chamber was evacuated to 0.5 Pa. High purity nitrogen gas was introduced into the chamber. The specimen was heated up to a holding temperature at a specified pressure. This temperature was monitored by thermocouples, which were embedded into the setup.

The nitriding process was performed in two steps. First, the pre-sputtering process was carried out for one hour or 3.6 ks using nitrogen gas with a 200 mL/min flow rate at 70 Pa. This process removes the oxide layer from the titanium surface and activates the nitrogen diffusion into the titanium matrix. In second, the nitriding process was carried out for 14.4 ks using the nitrogen and hydrogen gas mixture with the flow rate ratio of 160 for nitrogen to 40 mL/min for hydrogen. In this condition, the plasma was ignited by the RF voltage of 250 V and the dc bias voltage of –600 V at 35 Pa. The nitriding temperature was

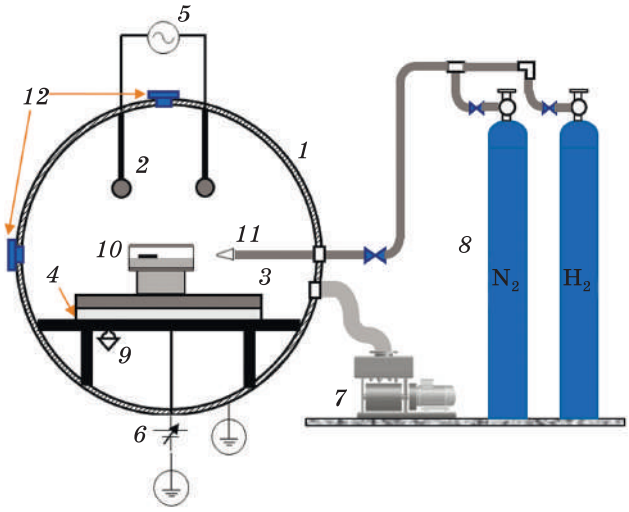


*Fig. 1.* The schematic design of the RF–DC plasma system with the cathode device: *1* — vacuum chamber; *2* — dipole electrode (anode); *3* — sample holder (cathode); *4* — resistive heater; *5* — RF-generator; *6* — DC-generator; *7* — vacuum pump; *8* — gas cylinders; *9* — thermocouple; *10* — hollow cathode setup; *11* — gas nozzle; *12* — view window

controlled to be 623, 673, and 723 K, respectively. After nitriding, the specimen was cooled down in the chamber under the nitrogen atmosphere.

After nitridation, specimens were cut into a size of 10 mm × 20 mm. The nitrided samples surfaces and cross-sections were polished with a grade of #150 to #2400 to have the maximum roughness below 0.1. Those pieces were analysed by a scanning electron microscope (FEI Quanta FEG 150) at Central Laboratory of Life Science in Brawijaya University. Their surface hardness was measured by a Vickers microhardness tester (Akashi MVK-H1). X-ray diffraction (XRD Rigaku SmartLab) with monochromatic Cu $K_\alpha$ radiation at a wavelength of 1.54060 Å was utilized for crystallographic analysis. The High-Score Plus version 3.0 software analysed the XRD diagrams and the ICSD reference data.

## 3. Obtained Results

### *3.1. Cross-Section Microstructure*

SEM was utilized to measure the compound layer thickness ($d$). Figure 2 compares the SEM image on the cross-sections of nitrided specimens at 623, 673, and 723 K for the coarse- and fine-grained samples.

As reported recently, compound layer formation through the nitriding process causes a significant increase in surface hardness [24]. The diffusion layer that appears as a dark area under the compound layer also supports an increase in surface hardness.

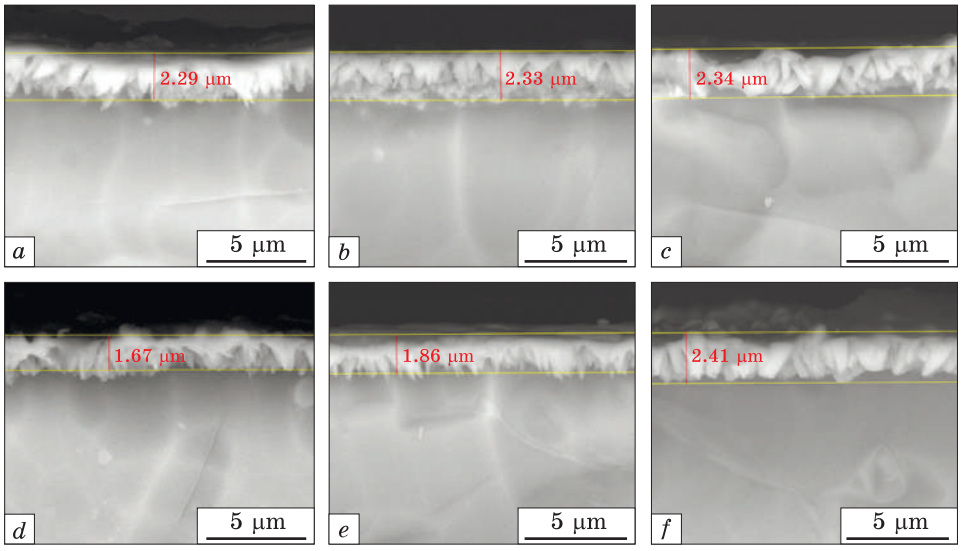


*Fig. 2*. SEM images on the cross-section of the nitrided titanium samples: 623 K (*a*), 673 K (*b*), 723 K (*c*) for the coarse-grained specimens, and 623 K (*d*), 673 K (*e*), and 723 K (*f*) for the fine-grained specimens

The compound layer thickness $d$ monotonously increased with increasing the holding temperature for both specimens [25]; *e.g.*, $d = 2.29$ μm at 623 K while $d = 2.34$ μm at 723 K, for coarse-grained titanium, and $d = 1.67$ μm at 623 K while $d = 2.41$ μm at 723 K for fine-grained titanium depicted in Fig. 2.

The success of the titanium nitriding process at low temperatures is determined by the synergistic relationship between the intensification of nitrogen diffusion using a hollow cathode and the phase transformation forming the compound layer [23, 26]. The addition of a hollow cathode device to the glow discharge plasma operated at an RF voltage of 250 V and a DC bias voltage of –600 V indicates a high concentration of nitrogen ion species [26]. These ions accelerated to impinge on the workpiece, bombard, and remove the oxide from the surface so the diffusion could be more effective, even at low temperatures [21]. The following section will discuss the mechanism of phase transformation through XRD observations.

### 3.2. Phase Composition of Untreated Titanium

Cp-Ti generally exhibits an h.c.p. crystal structure at low temperatures (α-Ti). On the untreated titanium plate used as the sample in this study, all XRD pattern peaks showed the hexagonal α-Ti of $P6_3/mmc$. Table 1 shows differences in the crystal lattice parameters on the coarse-grained and fine-grained Cp-Ti grade 2 plates, which refer to the obtained XRD data based on the reference of ICSD 98-007-6265 and ICSD 98-005-3784. The XRD pattern analysis results show that coarse-grained and fine-grained have a similar hexagonal structure. Still, the fine-grained titanium shows a larger lattice constant and smaller density when compared to the coarse-grained.

*Table 1.* **Crystal lattice parameters of α-Ti on the untreated coarse-grained and fine-grained Ti plate refer to the XRD data**

| Parameter | Coarse-grained Ti | Fine-grained Ti |
|---|---|---|
| Crystal system | Hexagonal | Hexagonal |
| Space group | $P6_3/mmc$ | $P6_3/mmc$ |
| $a = b$, Å | 2.944 | 2.970 |
| $c$, Å | 4.678 | 4.720 |
| $c/a$ | 1.58899 | 1.58923 |
| Calculated density, g/cm$^3$ | 4.53 | 4.41 |
| Volume of cell, Å$^3$ | 35.11 | 36.06 |

### *3.3. Phase Composition of Nitrided Coarse-Grained Titanium*

In this section, we will explain how the mechanism of titanium phase changes due to nitrogen diffusion during the nitriding process from $N_2$–$H_2$ working gas with a flow rate of 160–40 mL/min in the 4 hours nitriding process at three different holding temperatures at 623, 673, and 723 K for coarse-grained titanium samples. The XRD patterns of each piece carried out the analysis results before and after the nitriding process. Fig. 3 showed the XRD diffractogram of untreated and the nitrided coarse-grained titanium after the 4 hours process in the RF–DC plasma system with the hollow cathode device.

The XRD observations did not show any α-Ti phase shift for all samples. The condition is similar to the Ti–6Al–4V nitriding study report, which stated no line shift in the α-phase for all changes in process parameters [21]. However, they found the line shift occurred in the β-phase. In the present investigation, only three α-Ti planes still ap-

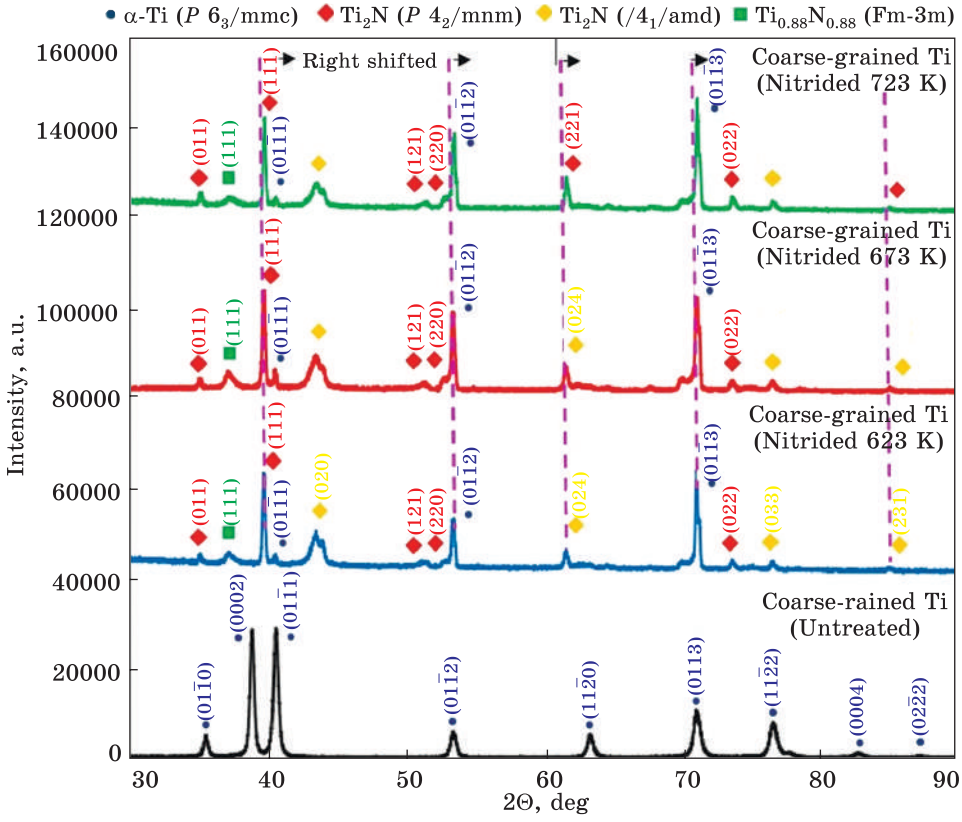


*Fig. 3.* The XRD diffractograms of the untreated coarse-grained titanium samples were compared with the nitrided coarse-grained titanium samples at 623, 673, and 723 K, respectively

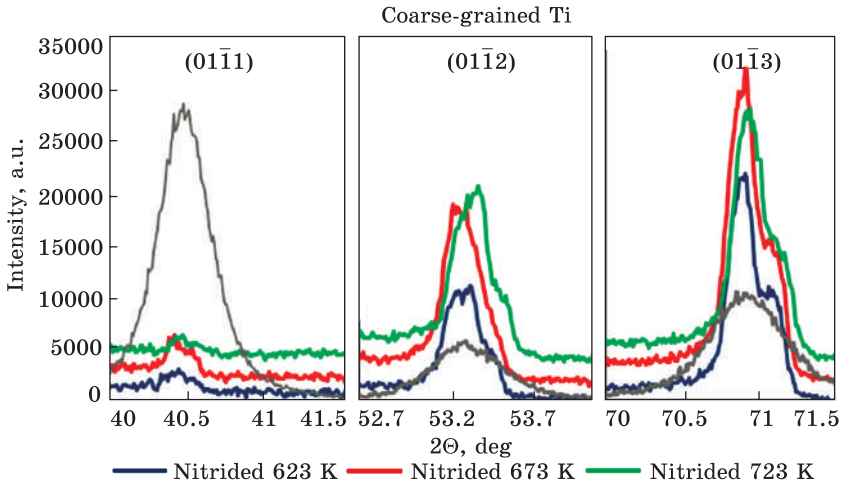


*Fig. 4*. The XRD diffractograms of α-Ti peak observed in untreated coarse-grained Ti and after nitriding process at 623, 673, and 723 K, respectively

pear in the form of prismatic planes (01$\bar{1}$1), (01$\bar{1}$2) and (01$\bar{1}$3) as shown in Fig. 4.

Several phases are formed as a surface layer, which increases the surface hardness of the nitrided titanium. These phases occur due to the redistribution of the h.c.p. structure of α-Ti after interstitial diffusion of nitrogen atoms in the titanium crystal lattice to form a new phase of $Ti_2N$, which has a tetragonal structure, and TiN which has a cubic structure. The XRD pattern in Figure 4 depicted the nitrided coarse-grained titanium samples with solid solution phase according to the chemical formula of $Ti_{0.83}N_{0.17}$ with the space group of $P6_3/mmc$. Moreover, there are two phases of $Ti_2N$, indicated by the space group of $P4_2/mnm$ and $I4_1/amd$. It also detected the $Ti_{0.88}N_{0.88}$ phase with a space group of $Fm\text{-}3m$. All of the lattice parameters showed in Table 2.

*Table 2*. **Crystal lattice parameters of the new phase on the nitrided coarse-grained titanium plate referring to the XRD data**

| Parameter | (1) | (2) | (3) | (4) |
|---|---|---|---|---|
| | $Ti_{0.83}N_{0.17}$ phase | δ-$Ti_2N$ phase | ε-$Ti_2N$ phase | $Ti_{0.88}N_{0.88}$ phase |
| Crystal system | Hexagonal | Tetragonal | Tetragonal | Cubic |
| Space group | $P6_3/mmc$ | $I4_1/amd$ | $P4_2/mnm$ | $Fm\text{-}3m$ |
| $a = b$, Å | 2.969 | 4.140 | 4.945 | 4.220 |
| $c$, Å | 4.777 | 8.805 | 3.034 | 4.220 |
| $c/a$ | 1.60896 | 2.12681 | 0.61355 | — |
| Calculated density, g/cm$^3$ | 3.84 | 4.83 | 4.91 | 4.41 |
| Volume of cell, Å$^3$ | 36.47 | 150.91 | 74.19 | 36.06 |

In the nitriding process on coarse-grained titanium samples, almost all α-Ti peaks are suppressed due to phase changes. There are only two peaks in the lattice plane $(01\bar{1}2)$ and $(01\bar{1}3)$. Nitrogen atoms were diffused interstitially into the titanium crystal lattice to form a solid solution if the nitrogen concentration was below 9.0 at.%. The x-ray diffraction pattern at 2θ of 69.8° (in the nitrided samples) shows the hexagonal structure of $Ti_{0.83}N_{0.17}$. For higher nitrogen concentration, the tetragonal structure of δ-$Ti_2N$ phase will begin to form in the space group of $I4_1/amd$. The peaks at 43.2° and 43.8° diffracted from the same crystal plane (020) represent the δ-$Ti_2N$ phase. This structure is a metastable phase of $Ti_2N$ obtained by increasing nitrogen concentration during the nitriding process. Reconstruction will form a stable ε-$Ti_2N$ with the *c* value of 3.034 Å, which was a significant change from the *c* value.

Different process temperatures affect the anisotropic phase transformation of the hard surface layer of the $Ti_2N$ and TiN precipitation. The increasing holding temperatures influence the dynamics of the phase transformation that occurs. Some peaks in the XRD pattern appear to shift slightly to the right when the nitriding temperature increases. It indicates a reconstruction of the crystal structure during the formation process of titanium nitride phases. At the nitriding temperature of 623 K and 673 K, it found two peaks at 2θ of 61.36° and 84.2° indicate the space group of $I4_1/amd$. However, at 723 K, the slight shifts to 2θ of 61.43° and 84.7° showed the space group of $P4_2/mnm$. The existence of a right shift peak indicates that the crystal lattice is getting smaller due to stress by nitrogen diffusion for the increasing nitriding temperature, and going along with it, the surface hardness is increased for the higher the nitriding temperature.

In the nitriding process of coarse-grained titanium samples, the dominant produced phase is $Ti_2N$. The stable ε-$Ti_2N$ phase is a transformation that results from the δ-$Ti_2N$ due to the reconstruction process with increasing nitrogen concentrations. A peak of cubic structure in (111) plane at 2θ of 37.1° indicates the formation of $Ti_{0.88}N_{0.88}$ compound with a space group of $Fm\text{–}3m$.

### *3.4. Phase Composition of Nitrided Fine-Grained Titanium*

The nitriding process with the same parameters was also carried out on fine-grained titanium samples. We use the MDF fine-grained titanium grade 2 as the sample in this process. The aim was to study the effect of grain size on the effectiveness of the nitriding process for titanium at low temperatures. It also determines whether there is a difference in the structure of the nitrided titanium. Figure 5 depicted the XRD diffractograms of the untreated fine-grained titanium compared to the nitrided samples at 623, 673, and 723 K, respectively.

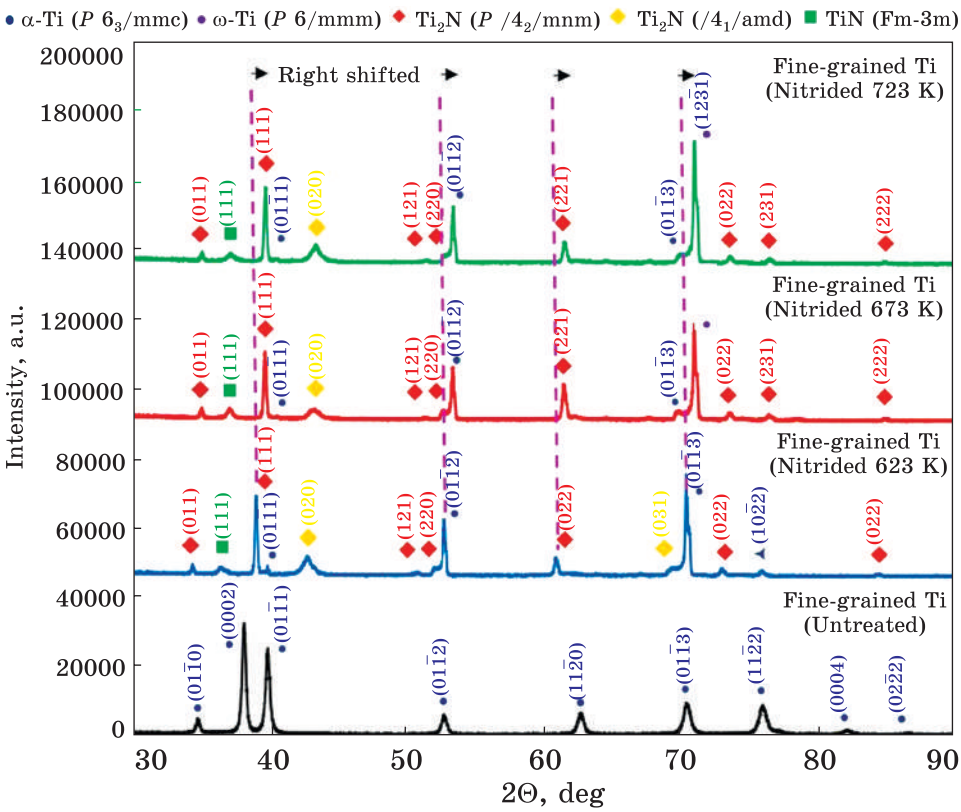


*Fig. 5*. The XRD diffractograms of the untreated fine-grained titanium samples were compared with the nitrided fine-grained titanium samples at 623, 673, and 723 K, respectively

In general, the surface-layer formation process obtained in fine-grained titanium samples is the same as coarse-grained titanium. However, there was a slightly different size of the α-Ti crystal lattice after the nitriding process. It found a slight peak shift of α-Ti phase on the 2θ of 52.6° before nitriding to 53.2° after nitrided at a temperature of 673 and 723 K. The α-Ti crystal lattice constants reduce from the value of 2.97 to 2.95 Å in the *a* and *b* axis and reduce from 4.72 to 4.68 Å in the *c* axis after the nitriding process (Table 1 and Table 3). It was an indication that fine-grained titanium crystals are more prone to rearranging their crystal structure. The ω-Ti phase was formed at the 673 and 723 K nitriding temperatures in the peak with 2θ of 70.87°. In the nitriding process, the specimen will be exposed to a compressive force from bombarding titanium atoms by high-energy plasma species. This situation allows the emergence of torque force that can cause shearing stress. This shear stress is highly possible to trigger phase transformation from α-Ti to ω-Ti [27]. This transformation allows the diffusion

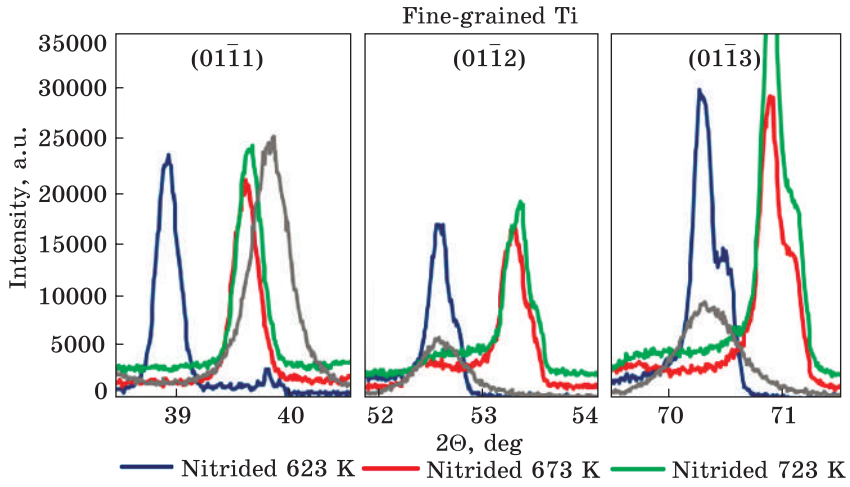


*Fig. 6*. The XRD diffractograms of α-Ti peak observed in untreated fine-grained Ti and after nitriding process at 623, 673, and 723 K, respectively

process to occur more effectively because the void space in ω-Ti is more considerable than α-Ti.

The XRD pattern results for fine-grained titanium samples show the effect of process temperature on the titanium-nitride phase formation. The change in the phase formation pattern occurs at a temperature change from 623 to 673 K. The same phase of the titanium nitride detects at a temperature change from 673 to 723 K. However, a more compact structure visible at a process temperature of 723 K, characterized by a shift of the peak to the right in the XRD pattern. Moreover, the right peak shift is more significant in the fine-grained samples than in the coarse-grained samples, as shown in Fig. 5.

Similar to the XRD pattern observed in the coarse-grained samples, the same α-Ti planes were observed in the fine-grained samples, but shifts occurred at the process temperatures of 673 and 723 K described in Fig. 6.

Several peaks at 34.3°, 38.9°, and 50.7° showed $Ti_2N_{0.8}$ compound at 623 K nitriding temperature. While at 673 and 723 K, the different compound of ε-$Ti_2N$ in the 2θ of 34.9°, 39.6°, and 52.5° was detected. Another phase difference occurred at a peak in the 2θ of 75.7° that indicates α-Ti in the plane (01$\bar{1}$3) at 623 K process temperature. Meanwhile, in the temperature process of 673 and 723 K, a ε-$Ti_2N$ peak with a space group $P\ 4_2/mnm$ was detected at 2θ 76.3°.

When the nitriding temperature increased from 623 K to 673 K, several peaks with the same space groups and crystal planes were also proven with different Ti and N compositions. At nitriding temperature 623 K, there is obtained $TiN_{0.61}$ represented by peak 43.1°. However,

*Table 3.* **Crystal lattice parameters of the new phase on the nitrided fine-grained titanium plate refer to the XRD data**

| Parameter | (1) | (2) | (3) | (4) |
|---|---|---|---|---|
| | α-Ti phase | ω-Ti phase | $TiN_{0.61}$ phase* | δ-$Ti_2N$ phase |
| Crystal system | Hexagonal | Hexagonal | Tetragonal | Tetragonal |
| Space group | $P6_3/mmc$ | $P6/mmm$ | $I4_1/amd$ | $I4_1/amd$ |
| $a = b$, Å | 2.951 | 4.600 | 4.198 | 4.150 |
| $c$, Å | 4.679 | 2.820 | 8.591 | 8.801 |
| $c/a$ | 1.58556 | 0.61304 | 2.04645 | 2.12072 |
| Calculated density, g/cm³ | 4.51 | 4.62 | 4.95 | 4.81 |
| Volume of cell, Å³ | 35.29 | 51.68 | 151.40 | 151.58 |

| Parameter | (5) | (6) | (7) | (8) |
|---|---|---|---|---|
| | $Ti_2N_{0.8}$ phase* | ε-$Ti_2N$ phase | $Ti_{0.88}N_{0.88}$ phase* | TiN phase |
| Crystal system | Tetragonal | Tetragonal | Cubic | Cubic |
| Space group | $P4_2/mnm$ | $P4_2/mnm$ | $Fm\text{-}3m$ | $Fm$-3m |
| $a = b$, Å | 4.981 | 4.945 | 4.220 | 4.234 |
| $c$, Å | 3.059 | 3.034 | 4.220 | 4.234 |
| $c/a$ | 0.61413 | 0.61355 | — | — |
| Calculated density, g/cm³ | 4.68 | 4.91 | 4.82 | 5.41 |
| Volume of cell, Å³ | 75.89 | 74.19 | 75.15 | 75.90 |

* Titanium nitride phase found at temperature process of 623 K

ε-$Ti_2N$ compound 43.2° found at 673, and 723 K. Similar indication occurs in the cubic phase of TiN in the crystal plane (111) with the space group $Fm\text{-}3m$. $Ti_{0.88}N_{0.88}$ compound formed at 623 K, and the $Ti_1N_1$ formed at 673 and 723 K. The $Ti_1N_1$ phase shows a more significant lattice parameter and a higher density than the $Ti_{0.88}N_{0.88}$ phase, as seen in Table 3. That indicator shows the higher nitrogen content in titanium crystals causes structural reconstruction, so the Ti–N bonds expand. A unique phenomenon exhibits in the temperature rise during the nitriding process.

## 4. Discussion

The interstitial diffusion process in the h.c.p. α-Ti crystals by the nitrogen atom with the concentration of 0–9 at.% in the octahedral void (interstice) will form a solid solution α-(N)Ti or $TiN_x$. For concentration up to 22 at.%, there has been a saturation condition of the α-(N)Ti solid solution, and there will be cooperative deformation of the titanium lattice [28]. The compound layer formed on the titanium surface has been the major factor in the hardening process [29, 30].

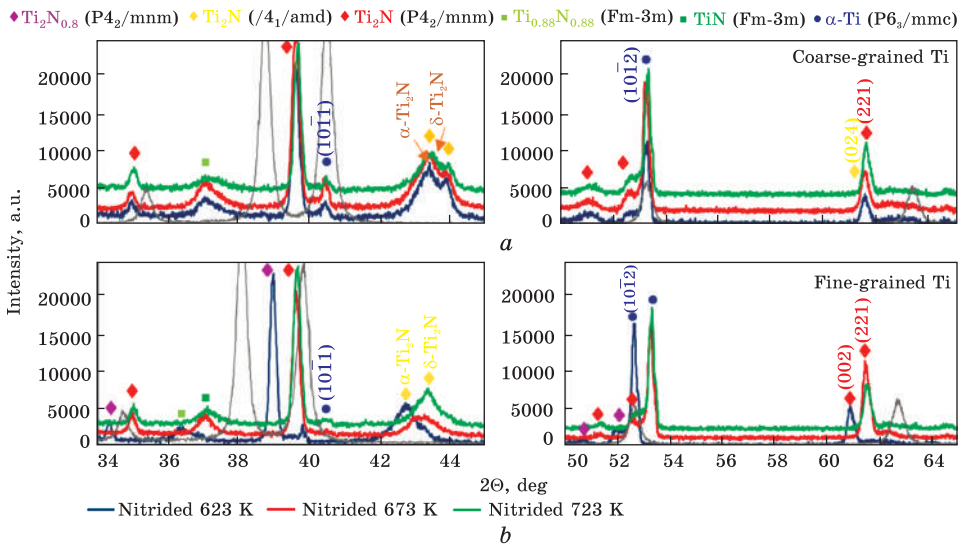


*Fig. 7.* The XRD pattern differences of structural phase transformation of α-Ti (grey colour online) in coarse-grained Ti (*a*) and fine-grained Ti (*b*) at three different holding temperatures: 623, 673, and 723 K, respectively

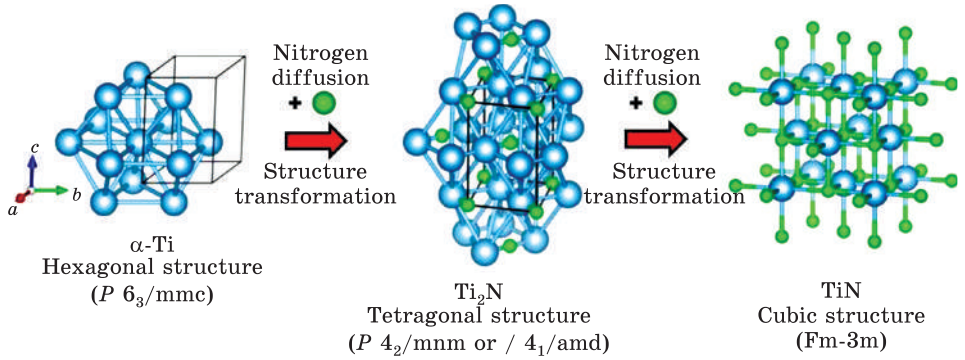


*Fig. 8.* The α-Ti structure transformation forms the surface layer of $Ti_2N$ and TiN during the nitriding process

Intensification of plasma nitrogen ions proved the formation of a compound layer even though the plasma nitriding process was carried out at low temperatures using a hollow cathode. On the other hand, a transformation will produce the $Ti_2N$ and TiN phases due to the structure's rearrangement. It appears that the grain size of the titanium sample also greatly influences the anisotropic formation of the compound layer. The layer's formation occurs at different holding temperatures, *i.e.*, 623, 673, and 723 K. The anisotropic phase transformation process is more evident in the nitriding carried out on the fine-grain titanium sample. Figure 7 illustrates the differences of XRD pattern changes for the formation of

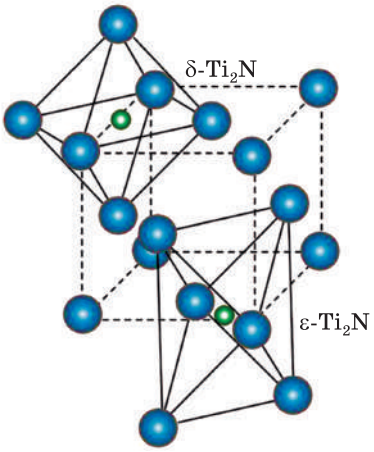


*Fig. 9.* The arrangement of Ti and N atom in δ-$Ti_2N$ and ε-$Ti_2N$ structure

$Ti_2N$ and $Ti_xN_x$ on coarse-grained and fine-grained titanium samples.

In general, the formation, development, and reconstruction of the preferred orientations and growth of the nitride surface layer consist of $Ti_2N$ and TiN depicted in Fig. 8.

The crystallization of titanium nitride to obtain the cubic structure of TiN has a wide range of compositions from $TiN_{0.42}$ to $TiN_{1.02}$. The crystallization is affected by the N concentration that forms Ti and N bonds. A limited N concentration, initially, in $TiN_x$ with $0.5 < x < 0.6$, will be developed that creates a tetragonal structure known as the metastable phase δ-$Ti_2N$. Higher nitrogen concentration will come into a stable ε-$Ti_2N$ phase. Each N atom is surrounded by six titanium atoms in both structures in a distorted octahedral position with two Ti atoms at a slightly smaller N–Ti distance than the other four atoms [31]. In the δ-$Ti_2N$ structure, the nitrogen atom is placed at a position (0, 1/2, 0), while in the ε-$Ti_2N$ structure, the nitrogen atom at the centre of the octahedral structure deforms at position (3/4, 1/4, 0). This structure has narrower spacing between the lattices and the typical octahedral structure. The Ti atoms adjacent to the N atoms experience a shift to form a tetragonal lattice structure with a smaller axis ratio. The strong covalent bonds formed between Ti and N atoms give a stable structure [32]. Ti and N atoms' arrangement in δ-$Ti_2N$ and ε-$Ti_2N$ is depicted in Fig. 9. After the formation of $Ti_2N$, the increasing nitrogen concentration in the system will cause a reconstruction of the structure. The high density of nitrogen ions in $N_2$–$H_2$ plasma will drive the formation of TiN precipitate on the titanium surface.

We propose the phase transformation mechanism of α-Ti during the nitriding process as follows. In the first step, nitrogen atoms diffuse interstitially to an α-Ti lattice and form the α-Ti–N solid solution. The second step is the formation of δ-$Ti_2N$ and ε-$Ti_2N$. This nitride surface layer is formed at the top layer, where the underneath layer is the diffusion zone of α-Ti–N. Due to the negative $\Delta H_f$ of $Ti_2N$ (15 kJ/mole) the phase formation of $Ti_2N$ is inevitable due to the provided kinetic energy and nitrogen concentration. In this step, ε-$Ti_2N$ is not formed directly. It occurs through the transformation from metastable δ-$Ti_2N$ to stable ε-$Ti_2N$ through a compacting process on the *c* axis. Another surface transformation would occur by progressing nitrogen diffusion until its con-

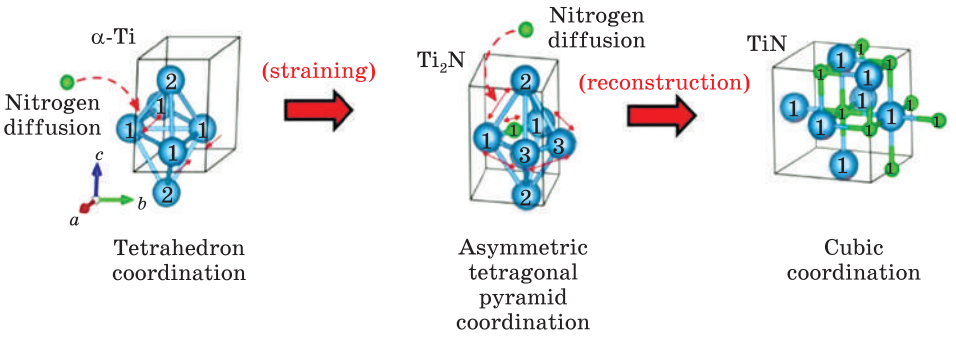


*Fig. 10*. The nitrogen transfer mechanism against α-Ti crystals form $Ti_2N$ and TiN phases in the nitriding process

centration reaches more than needed δ-TiN formation. In this condition, ε-$Ti_2N$ will transform to δ-TiN [33]. According to the Ti–N equilibrium diagram, the dispersed δ-TiN precipitates are formed in the region where the nitrogen concentration exceeds the solubility limit [32, 34].

The nitrogen transfer mechanism in the nitriding process against α-Ti crystals to form $Ti_2N$ and TiN phases are summarized in Fig. 10. The phase change in the nitriding process starts from the h.c.p. α-Ti structure to the tetragonal structure owned by $Ti_2N$. Diffusion of nitrogen atoms into the α-Ti bonds them in tetrahedron co-ordination. The Ti position change forms the new composition of the asymmetrical tetragonal pyramid due to the Ti position change. It will cause the expansion of the Ti–Ti bonds when they are interstice with nitrogen. The nitrogen diffusion exerts a repulsive force and compresses the other Ti–Ti bonds. The increasing nitrogen concentration in the increasing holding temperature will stimulate a chemical reaction between Ti and N, which is indicated by generating a new TiN phase.

The formation mechanism of ε-$Ti_2N$ stable structure starting from the asymmetric δ-$Ti_2N$ structure is characterized by stretching the titanium lattice in the c axis to about 8.8 Å and increasing the phase density. The structure rearrangement is marked by compacting the structure to form a more stable ε-$Ti_2N$ structure with a cell volume that is only about half of the cell volume of δ-$Ti_2N$ phase structure and is accompanied by an increase in phase density. Due to the increase of nitrogen concentration during temperature holding time, the reconstruction process will continue until the achieving of stoichiometric equilibrium. An asymmetric tetragonal pyramid structure of $Ti_2N$ was rearranged to TiN with a more symmetrical and stoichiometric cubic coordination. Besides, in these coarse-grained samples, the cubic structure is found with the chemical formula of $Ti_{0.88}N_{0.88}$. Generally, the phase transformation depends on the plasma condition and process parameter, mainly due to low pressure and increased temperature.

## 5. Conclusions

The nitriding process has systematically studied the effect of titanium grain size on forming the surface layer. The low temperatures process utilizes high-density RF–DC plasmas, with a hollow cathode device significantly affecting the nitride phase transformation. The phase transformation in the surface layer begins with forming α-Ti–N solid solution. The preceded process shows the change of δ-$Ti_2N$ to ε-$Ti_2N$ due to the displacive transformation of tetragonal coordination. In addition, it was followed by the formation of cubic coordination of TiN through the reconstruction of the Ti–N bonds.

The result shows the anisotropic phase transformation on the surface layer of titanium in different process temperatures. The titanium nitride phase of the $Ti_2N$ and TiN phases at 673 and 723 K temperature process is more stable than at 623 K. The increased process temperature to 723 K obtained the peak shift to the right in the XRD pattern, where a more significant shift occurs in the fine-grained titanium sample. This shift indicates more compacting crystals that cause a higher surface hardness than coarse-grained ones. The use of fine-grained titanium proved the more effective diffusion in the nitriding process due to the formation of stable $Ti_2N$ and TiN.

**Acknowledgements.** The authors thank Surface Engineering Design Laboratory, Shibaura Institute of Technology, Ota-City, Tokyo, Japan, for research facilities, and Shibaura Institute of Technology, Tokyo, Japan, for providing all the tools for analysing research data. The authors are grateful for the research funding Brawijaya University for financial support through "Program Hibah Guru Besar dan Doktor Tahun Anggaran 2021" with the contract number: 1595/UN10.F09/PN/2021, provided by Brawijaya University, Malang, Indonesia.

REFERENCES

1. G. Suzuki, M. Hirota, N. Hoshi, K. Kimoto, H. Miura, M. Yoshinari, T. Hayakawa, and Ch. Ohkubo, Effect of surface treatment of multi-directionally forged (MDF) titanium implant on bone response, *Metals*, **9**, No. 2: 230 (2019); https://doi.org/10.3390/met9020230
2. A.M. Khorasani, M. Goldberg, E.H. Doeven, and G. Littlefair, Titanium in biomedical applications — properties and fabrication: a review, *J. Biomater. Tissue Eng.*, **5**, No. 8: 593–619 (2015); https://doi.org/10.1166/jbt.2015.1361
3. S.J. Gobbi, V.J. Gobbi, G. Reinke, and Y. Rocha, Orthopedic implants: coating with TiN, *Biomed. J. Sci. Tech. Res.*, **16**, No. 1: 11740–11742 (2019); https://doi.org/10.26717/BJSTR.2019.16.002786
4. M. Pilarska, T. Frączek, and K. Maźniak, The role of complementary potential in plasma nitriding progress of technical titanium, *Arch. Metall. Mater.*, **63**, No. 4: 1637–1642 (2018); https://doi.org/10.24425/amm.2018.125087

5. S. Farè, N. Lecis, M. Vedani, A. Silipigni, and P. Favoino, Properties of nitrided layers formed during plasma nitriding of commercially pure Ti and Ti–6Al–4V alloy, *Surf. Coatings Technol.*, **206**, Nos. 8–9: 2287–2292 (2012); https://doi.org/10.1016/j.surfcoat.2011.10.006
6. A.M. Kamat, S.M. Copley, and J.A. Todd, Effect of processing parameters on microstructure during laser-sustained plasma (LSP) nitriding of commercially-pure titanium, *Acta Mater.*, **107**: 72–82 (2016); https://doi.org/10.1016/j.actamat.2016.01.051
7. H. Mora-Sanchez, I. Sabirov, M.A. Monclus, E. Matykina, and J.M. Molina-Aldareguia, Ultra-fine grained pure Titanium for biomedical applications, *Mater. Technol.*, **31**, No. 13: 756–771 (2016); https://doi.org/10.1080/10667857.2016.1238131
8. B. Ravisankar and J.K. Park, ECAP of commercially pure titanium: A review, *Trans Indian Inst. Met.*, **61**, No. 1: 51–62 (2008); https://doi.org/10.1007/s12666-008-0058-6
9. Y. Todaka, M. Umemoto, A. Yamazaki, J. Sasaki, and K. Tsuchiya, Effect of strain path in high-pressure torsion process on hardening in commercial purity titanium, *Mater. Trans.*, **49**, No. 1: 47–53 (2008); https://doi.org/10.2320/matertrans.ME200714
10. O. Unal, E. Maleki, and R. Varol, Effect of severe shot peening and ultra-low temperature plasma nitriding on Ti–6Al–4V alloy, *Vacuum*, **150**, 69–78 (2018); https://doi.org/10.1016/j.vacuum.2018.01.027
11. K. Topolski, W. Pachla, and H. Garbacz, Progress in hydrostatic extrusion of titanium, *J. Mater. Sci.*, **48**, No. 13: 4543–4548 (2013); https://doi.org/10.1007/s10853-012-7086-7
12. Y. Beygelzimer, V. Varyukhin, D. Orlov, B. Efros, V. Stolyarov, and H. Salimgareyev, Microstructural evolution of titanium under twist extrusion, *Ultrafine grained Material II* (Eds. Y.T. Zhu, T.G. Langdon, R.S. Mishra, S.L. Setniatin, M.J. Saran, and T.C. Lowe) (Wiley: 2002), pp. 43–46; https://doi.org/10.1002/9781118804537.ch5
13. M. Karimi, M.R. Toroghinejad, and J. Dutkiewicz, Nanostructure formation during accumulative roll bonding of commercial purity titanium, *Mater. Charact.*, **122**: 98–103 (2016); https://doi.org/10.1016/j.matchar.2016.10.024
14. S.V. Zherebtsov, G.S. Dyakonov, A.A. Salem, V.I. Sokolenko, G.A. Salishchev, and S.L. Semiatin, Formation of nanostructures in commercial-purity titanium via cryorolling, *Acta Mater.*, **61**, No. 4: 1167–1178 (2013); https://doi.org/10.1016/j.actamat.2012.10.026
15. W.J. Kim, S.J. Yoo, and J.B. Lee, Microstructure and mechanical properties of pure Ti processed by high-ratio differential speed rolling at room temperature, *Scr. Mater.*, **62**, No. 7: 451–454 (2010); https://doi.org/10.1016/j.scriptamat.2009.12.008
16. A. Farias, G.F. Batalha, E.F. Prados, R. Magnabosco, and S. Delijaicov, Tool wear evaluations in friction stir processing of commercial titanium Ti–6Al–4V, *Wear*, **302**, Nos. 1–2: 1327–1333 (2013); https://doi.org/10.1016/j.wear.2012.10.025
17. I. Ansarian, M.H. Shaeri, M. Ebrahimi, P. Minárik, and K. Bartha, Microstructure evolution and mechanical behaviour of severely deformed pure titanium through multi directional forging, *J. Alloys Compd.*, **776**, 83–95 (2019); https://doi.org/10.1016/j.jallcom.2018.10.196

18. V. Fouquet, L. Pichon, A. Straboni, and M. Drouet, Nitridation of Ti6Al4V by PBII: study of the nitrogen diffusion and of the nitride growth mechanism, *Surf. Coat. Technol.*, **186**, Nos. 1–2: 34–39 (2004); https://doi.org/10.1016/j.surfcoat.2004.04.006
19. A. Zhecheva, W. Sha, S. Malinov, and A. Long, Enhancing the microstructure and properties of titanium alloys through nitriding and other surface engineering methods, *Surf. Coatings Technol.*, **200**, No. 7: 2192–2207 (2005); https://doi.org/10.1016/j.surfcoat.2004.07.115
20. Y.S. Matychak, Specific kinetic features of nitriding of titanium caused by phase-structural transformations, *Mater. Sci.*, **48**, No. 5: 628–635 (2013); https://doi.org/10.1007/s11003-013-9547-9
21. E. Metin and O.T. Inal, Kinetics of layer growth and multiphase diffusion in ion- nitrided titanium, *Metall. Trans. A*, **20**, No. 9: 1819–1832 (1989); https://doi.org/10.1007/BF02663213
22. K. Farokhzadeh, J. Qian, and A. Edrisy, Effect of SPD surface layer on plasma nitriding of Ti–6Al–4V alloy, *Mater. Sci. Eng. A*, **589**: 199–208 (2014); https://doi.org/10.1016/j.msea.2013.09.077
23. T. Aizawa, Low temperature plasma nitriding of austenitic stainless steels, *Stainless Steels and Alloys* (Ed. Z. Duriagina) (InTech: 2018), pp. 31–50; https://doi.org/10.5772/intechopen.78365
24. D.J.D.H. Santjojo, M.S. Rajapadni, and S.P. Sakti, Nitriding of pure titanium by high density plasma using $H_2$–$N_2$ gas mixture at low temperature, *Int. J. GEOMATE*, **16**, No. 56: 141–146 (2019); https://doi.org/10.21660/2019.56.4697
25. I. Çelik and M. Karakan, Effect of plasma nitriding treatment on structural, tribological and electrochemical properties of commercially pure titanium, *Proc. Inst. Mech. Eng. Part H J. Eng. Med.*, **230**, No. 2: 145–152 (2016); https://doi.org/10.1177/0954411915621342
26. J.M. Windajanti, D.J.D.H. Santjojo, Abdurrouf, and M.A. Pamungkas, *Rom. J. Phys.*, **65**, No. 502: 1–13, 2020.
27. J.M. Windajanti, D.J.D.H. Santjojo, and A. Abdurrouf, Microstructure and phase transformation of pure titanium during nitriding process by high density plasma, *J. Sains Mater. Indones.*, **18**, No. 3: 116–122 (2017); https://doi.org/10.17146/jsmi.2017.18.3.4115
28. J.-P. Bars, D. David, E. Etchessahar, and J. Debuigne, Titanium α-nitrogen solid solution formed by high temperature nitriding: diffusion of nitrogen, hardness, and crystallographic parameters, *Metall. Trans. A*, **14**: 1537–1538 (1983); https://doi.org/10.1007/BF02654379
29. V.M. Fedirko and I.M. Pohrelyuk, Kinetics of thermodiffusion saturation of VT22 titanium alloy with nitrogen within the temperature range 800–950°C, *Mater. Sci.*, **49**, No. 2: 145–157 (2013); https://doi.org/10.1007/s11003-013-9594-2
30. A. Grill, A. Raveh, and R. Avni, Layer structure and mechanical properties of low pressure r.f. plasma nitrided Ti–6Al–4V alloy, *Surf. Coatings Technol.*, **43–44**, Pt. 2: 745–755 (1990); https://doi.org/10.1016/0257-8972(90)90017-7
31. R. Eibler, Electronic structure of epsilon-$Ti_2N$ and delta′-$Ti_2N$, *J. Phys. Condens. Matter*, **5**, No. 30: 5261–5276 (1993); https://doi.org/10.1088/0953-8984/5/30/006
32. S. Nagakura and T. Kusunoki, Structure of $TiN_x$ studied by electron diffraction and microscopy, *J. Appl. Crystallogr.*, **10**, No. 1: 52–56 (1977); https://doi.org/10.1107/s0021889877012795

33. H. Aghajani and M.S. Motlagh, Effect of temperature on surface characteristics of nitrogen ion implanted biocompatible titanium, *J. Mater. Sci. Mater. Med.*, **28–29**: 1–16 (2017);
https://doi.org/10.1007/s10856-016-5843-x
34. P. Vlcak, J. Drahokoupil, P. Vertat, J. Sepitka, and J. Duchon, Hardness response to the stability of a Ti(+N) solid solution in an annealed TiN/Ti(+N)/Ti mixture layer formed by nitrogen ion implantation into titanium, *J. Alloys Compd.*, **746**: 490–495 (2018);
https://doi.org/10.1016/j.jallcom.2018.02.301

Received 04.02.2022;
in final version, 09.02.2022

*Дж.М. Віндажанті*[1], *М.С. Раджападні*[1], *Д.Дж.Д.Х. Санджоджо*[1],
*М.А. Памунґкас*[1], *А. Абдурруф*[1], *Т. Айзава*[2]

[1] Катедра фізики, факультет математики та природничих наук,
Університет Бравіджая,
Джалан Ветеран Маланґ, Східна Ява, Індонезія

[2] Лабораторія інженерного проєктування поверхонь,
Технологічний інститут Шібаура,
Ота-Сіті, Токіо, Японія

## МЕХАНІЗМ АНІЗОТРОПНОГО ФАЗОВОГО ПЕРЕТВОРЕННЯ НА ГРУБО- ТА ДРІБНОЗЕРНИСТОМУ ЧИСТОМУ ТИТАНІ ЗА НИЗЬКОТЕМПЕРАТУРНОГО ПЛАЗМОВОГО АЗОТУВАННЯ

Досліджено процес азотування грубозернистого та дрібнозернистого чистого титану, що відбувається за методом різноспрямованого кування за температур у 623, 673 і 723 К. Процес проводили плазмою радіочастотного односпрямованого струму високої густини у поєднанні з пристроєм з порожнистою катодою прямокутньої форми. В результаті одержано значне збільшення твердости поверхні за підвищення температури витримки. Твердість поверхні збільшується за рахунок утворення поверхневого шару, який складається з δ-$Ti_2N$, ε-$Ti_2N$ і $Ti_xN_x$, що спостерігається за результатами Рентґенової дифракції. У цій роботі пояснюється механізм утворення поверхневого шару. Також спостерігається анізотропне фазове перетворення нітриду титану через зсув піків Рентґенової дифракції праворуч. Розсіяні атоми Нітроґену під час процесу азотування спричинюють зміну орієнтації кристалу через структурне перетворення метастабільної фази δ-$Ti_2N$ у стабільну ε-$Ti_2N$. Структурна реконструкція продовжується шляхом формування $Ti_xN_x$ для досягнення стехіометричної рівноваги. Більше ущільнення мікроструктури поверхні також досягається підвищенням температури азотування.

**Ключові слова:** плазмове азотування, низька температура, чистий титан, дрібнозернистий, анізотропне фазове перетворення.